

## Article

# A Study on the Effect of Alumina on the Morphology and Reduction Behavior of Sinter by In Situ Observation

Sang Gyun Shin <sup>1</sup>, Wan Ho Kim <sup>2</sup> and Dong Joon Min <sup>1,\*</sup>

<sup>1</sup> Department of Material Science and Engineering, Yonsei University, 50 Yonsei-Ro, Seodaemun-Gu, Seoul 038722, Korea; mang2ca@gmail.com

<sup>2</sup> POSCO, Technical Research Laboratories, Donghaean-ro, Nam-gu, Pohang-si 6261, Gyeongsangbuk-do, Korea; whokim@posco.com

\* Correspondence: chemical@yonsei.ac.kr; Tel.: +82-2-2123-2840

**Abstract:** The effects of Al<sub>2</sub>O<sub>3</sub> content on the morphology and reducibility of sinter were respectively investigated using confocal laser microscopy and thermogravimetric analysis at 1273 K under CO gas. To understand the effects of the sintering process, separate samples were prepared via the equilibrium and metastable reaction routes. In the equilibrium samples, the addition of Al<sub>2</sub>O<sub>3</sub> led to the formation of the silico-ferrite of calcium and alumino phase and a decrease in the reduction rate due to the lowered reactivity of iron oxide. In contrast, in the metastable samples, the reduction rate increased after the addition of 2.5 mass% Al<sub>2</sub>O<sub>3</sub>. The addition of Al<sub>2</sub>O<sub>3</sub> decreased the fraction of the liquid phase and increased the fraction of pores in the sample. As a result, the reduction rate is proportional to the Al<sub>2</sub>O<sub>3</sub> content owing to the changes in the sinter morphology. In determining the reduction rate of the sinter, the influence of the microstructure on the diffusion of the reducing gas is more significant than that of the interfacial chemical reaction due to the formation of the SFCA phase. The microstructure changes of the sinter with the addition of Al<sub>2</sub>O<sub>3</sub> and the corresponding reduction behaviors are further discussed.

**Keywords:** sintering; Al<sub>2</sub>O<sub>3</sub>; reduction; morphology; porosity



**Citation:** Shin, S.G.; Kim, W.H.; Min, D.J. A Study on the Effect of Alumina on the Morphology and Reduction Behavior of Sinter by In Situ Observation. *Metals* **2021**, *11*, 740. <https://doi.org/10.3390/met11050740>

Academic Editor: Francisco Paula Gómez Cuevas

Received: 12 April 2021

Accepted: 27 April 2021

Published: 29 April 2021

**Publisher's Note:** MDPI stays neutral with regard to jurisdictional claims in published maps and institutional affiliations.



**Copyright:** © 2021 by the authors. Licensee MDPI, Basel, Switzerland. This article is an open access article distributed under the terms and conditions of the Creative Commons Attribution (CC BY) license (<https://creativecommons.org/licenses/by/4.0/>).

## 1. Introduction

Sintering technology is the most common agglomeration process for diversifying iron oxides in the blast furnace process. It affects the operational stability and productivity of the blast furnace process. The amount of gangue and Al<sub>2</sub>O<sub>3</sub> content in the ore has gradually increased in recent years owing to the depletion of high-quality iron ore [1,2]. The increase in the sinter Al<sub>2</sub>O<sub>3</sub> content is known to have detrimental effects in the operation of the blast furnace, such as the lowering of the gas permeability, slag fluidity, and reducibility of sinter [3–5]. Therefore, the effective utilization of iron ore containing Al<sub>2</sub>O<sub>3</sub> as a sinter in blast furnaces has attracted attention.

Many investigations have been performed on the effect of Al<sub>2</sub>O<sub>3</sub> on the sinter properties and reduction behavior. The impact of Al<sub>2</sub>O<sub>3</sub> on physical properties of sinter increases the viscosity of the primary melts [6,7] and decreases the strength of the sinter [8,9]. Additionally, the silico-ferrite of calcium and alumino (SFCA) phase has been observed in sinter with high contents of Al<sub>2</sub>O<sub>3</sub> [10–15] and influences the reduction behavior of sinter. On the base of equilibrium phase, Manzanek et al. [16] and Liao and Guo [17] conducted reduction studies on the influence of Al<sub>2</sub>O<sub>3</sub> on the sinter. Manzanek et al. [16] reported that sinter with 7 mass% Al<sub>2</sub>O<sub>3</sub> formed brownmillerite, which decreased the reducibility, but 3CaO·FeO·7Fe<sub>2</sub>O<sub>3</sub> and CaO·Al<sub>2</sub>O<sub>3</sub>·2Fe<sub>2</sub>O<sub>3</sub> phases were formed at 12 mass% Al<sub>2</sub>O<sub>3</sub>, which improved the reduction behavior. Liao and Guo [17] studied the effects of adding Al<sub>2</sub>O<sub>3</sub> on the reduction behavior in a sintered composition of the equilibrated SFCA phase and reported that the reduction rate of the SFCA phase was slower than that of hematite. However, because a metastable phase is formed in the typical sintering process, the elucidation

of the reduction behavior from equilibrium phase studies is limited. Research on the effects of  $\text{Al}_2\text{O}_3$  on the reduction behavior of sinters based on the metastable phase has also been reported, but research is still inadequate. Hessien et al. [18] reported that the reduction rate of the sinter increased or decreased depending on whether the SFCA phase was formed by the addition of  $\text{Al}_2\text{O}_3$ . Zeng et al. [19] also reported that the initial reduction rate increased with the addition of  $\text{Al}_2\text{O}_3$ , but the formation of the  $\text{FeAl}_2\text{O}_4$  phase later in the reduction stage retarded the reduction rate. However, these research results are not sufficient to confirm the effect of  $\text{Al}_2\text{O}_3$  on the reduction behavior because the metastable phases were not prepared in accordance with the temperature patterns of the sintering process.

Therefore, the present study focuses on the sinter microstructure and its reduction behavior during the sintering process. Metastable samples were prepared by simulating the sintering process, and equilibrium samples prepared for comparison. The influence of  $\text{Al}_2\text{O}_3$  content on the reducibility of the sinter was investigated at 1273 K using thermogravimetric analysis (TGA) under CO gas. The morphology changes in the sinter due to the addition of  $\text{Al}_2\text{O}_3$  and the corresponding reduction behavior are discussed in detail.

## 2. Materials and Methods

### 2.1. Sample Composition

Reagent-grade  $\text{CaCO}_3$  was calcined at 1273 K for 24 h to prepare CaO, which was mixed with reagent-grade  $\text{Fe}_2\text{O}_3$ ,  $\text{SiO}_2$ , and  $\text{Al}_2\text{O}_3$  powder according to the chemical compositions shown in Table 1.

**Table 1.** Chemical compositions of the equilibrium and metastable samples with various  $\text{Al}_2\text{O}_3$  contents.

Sample	Chemical Composition (mass%)				
	$\text{Fe}_2\text{O}_3$	CaO	$\text{SiO}_2$	$\text{Al}_2\text{O}_3$	Total
0 mass% $\text{Al}_2\text{O}_3$	85.0	10.0	5.0	0	100
2.5 mass% $\text{Al}_2\text{O}_3$	82.5	10.0	5.0	2.5	100
5 mass% $\text{Al}_2\text{O}_3$	80.0	10.0	5.0	5.0	100
10 mass% $\text{Al}_2\text{O}_3$	75.0	10.0	5.0	10	100

### 2.2. Characterization Techniques

The samples were prepared as equilibrium and metastable samples. In the equilibrium samples, the equilibrium phase was formed without microstructural effects, while in the metastable samples, the metastable phase was formed by simulating the sintering process temperature, which changed the microstructure accordingly. Each of the equilibrium samples (Figure 1a) was melted for 5 h at 1823 K in a Pt crucible and then quenched to room temperature. The sample was then crushed and sieved into particles 75–100  $\mu\text{m}$  in size. The crushed sample was again annealed at 1623 K (sintering temperature) in an air atmosphere for 24 h to form the equilibrium phase and then quenched, crushed, and sieved into particles 75–100  $\mu\text{m}$  in size. The crushed sample was pressed in a cylindrical mold (diameter: 13 mm) under a pressure of 3770  $\text{kgf}/\text{cm}^2$  to minimize the microstructural effect in the sample. The metastable samples were prepared by simulating the sintering temperature reported by Loo et al. [13]. A Pt crucible (diameter: 13 mm) containing a sample (Table 1) was placed on the confocal laser microscopy (Figure 2, CLM, VL2000DX-SVF17SP, Lasertec, Yokohama, Japan). As shown in Figure 1b, the temperature was increased from room temperature to 1073 K at 2 K/s and then to 1623 K at 20 K/s under air condition. The temperature was maintained at 1623 K for 120 s to form a metastable phase and cooled to 676 K at  $-2$  K/s, then quenched to room temperature. A reduction experiment was conducted without crushing the prepared sample to confirm the influence of the microstructure.

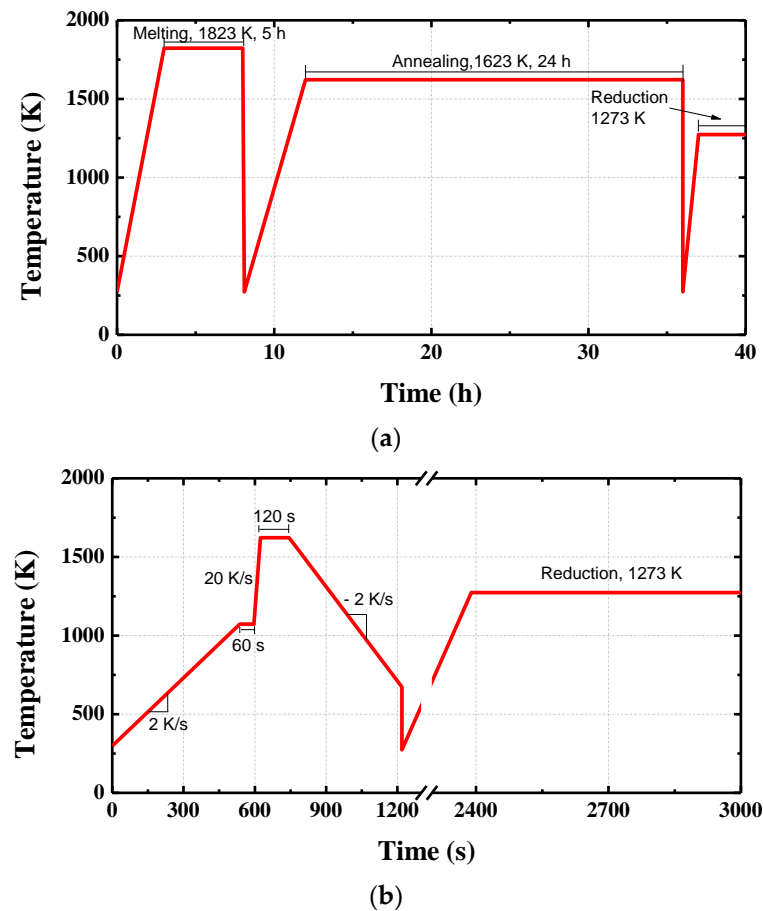


**Figure 1.** Temperature profiles of the preparation procedure: (a) equilibrium samples, (b) metastable samples.

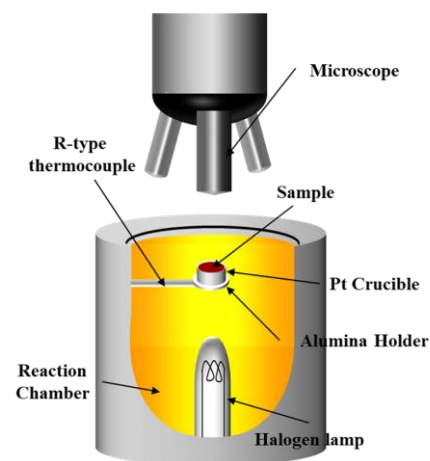


**Figure 2.** Schematic diagram of the confocal laser microscopy (CLM) setup.

### 2.3. Reduction Conditions and Analysis

Each sample (mass: 1.6 g) was hung on a Mo wire and loaded into a thermogravimetric analyzer (TGA, SETSYS Evolution, Setaram, Caluire-et-Cuire, France) and then heated (50 K/min) to 1273 K in a high-purity Ar (99.999%) atmosphere. When the temperature was achieved, Ar gas was replaced with CO gas (99.99%), and the weight changes were measured every second using TGA. Based on a preliminary experiment, the reducing gas flow was set at 500 cm<sup>3</sup>/min to minimize the gas-phase mass transfer of CO gas from the

gas stream to the surface of the solid particle. Using the obtained TGA experimental data, the reduction degree (R.D) was calculated as:

$$\text{R.D}(\%) = \frac{\Delta W_O^t}{W_O^i} \times 100, \quad (1)$$

where  $W_O^i$  is the amount of removable oxygen in the initial sample and  $\Delta W_O^t$  is the weight of oxygen removed at time  $t$ . The value of  $W_O^i$  is the amount of oxygen present in  $\text{Fe}_2\text{O}_3$ , assuming that only oxygen present in iron oxide is removed during the reduction process. X-ray diffraction was used for the phase analysis of the sample, and the porosity of the sample was analyzed using a mercury porosimeter (PM33GT, Quamtachrome, Graz, Austria).

### 3. Results and Discussion

#### 3.1. Influence of $\text{Al}_2\text{O}_3$ on the Reduction Behavior of Sinter

The effects of  $\text{Al}_2\text{O}_3$  on the reduction behavior of the equilibrium and metastable samples by CO gas at 1273 K are shown in Figure 3. In the equilibrium samples, the reduction rate decreases with increasing  $\text{Al}_2\text{O}_3$  content in the sinter. In the metastable samples, the reduction rate increases with the  $\text{Al}_2\text{O}_3$  content in the sinter. The reduction rates of the metastable samples are higher than those of the equilibrium samples.

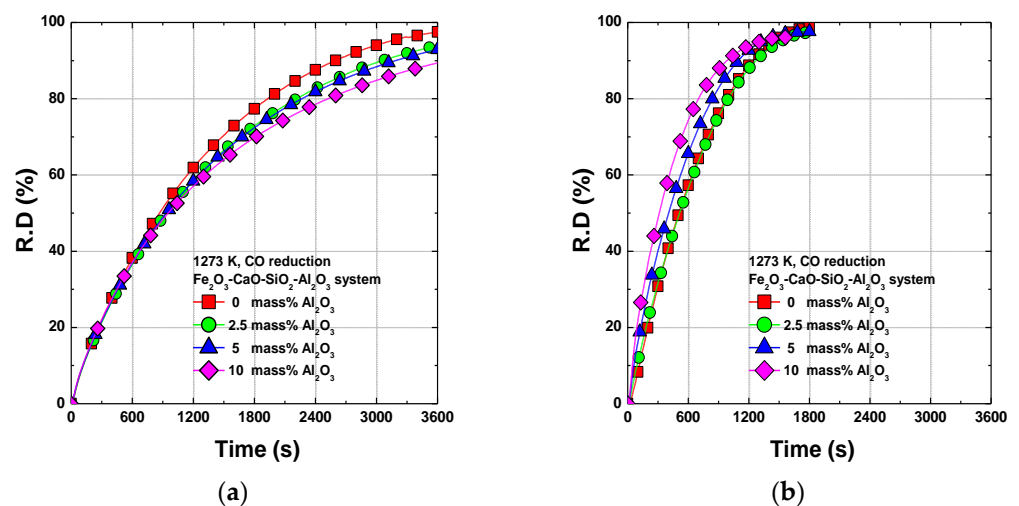


**Figure 3.** Reduction behavior of sinter with various  $\text{Al}_2\text{O}_3$  contents at 1273 K under CO gas: (a) equilibrium samples, (b) metastable samples.

The grain model that can analyze the gas–solid reaction for a cylindrical pellet proposed by Szekely [20] was used to analyze the reduction behavior of the sinter (Figure 3) in detail. In the heterogeneous gas–solid reaction model, the interfacial chemical reaction (ICR) rate constant is defined by:

$$g_{F_g}(X) = 1 - (1 - X)^{\frac{1}{2}} = k_2 \cdot \tau. \quad (2)$$

The rate constant of the gaseous mass transport (GMT) through the generated layer of the cylindrical compact is defined by:

$$p_{F_g}(X) = X + (1 - X) \ln(1 - X) = k_1 \cdot \tau. \quad (3)$$

The rate constant of the mixed control is defined by:

$$g_{F_g}(X) + \sigma^2 p_{F_g}(X) = k_{\text{mixed}} \cdot \tau. \quad (4)$$

In Equations (2)–(4),  $g_{F_g}$  and  $p_{F_g}$  are the conversion functions, and  $X$  is the reduction degree at a given time  $\tau$ .  $\sigma$  is the gas–solid reaction modulus. In a general gas–solid reaction, the  $\sigma$  value represents 1.  $k_1$ ,  $k_2$  and  $k_{\text{mixed}}$  are the apparent rate constants of the GMT through the product layer, the ICR, and the mixed control, respectively. If the conversion functions in Equations (2) and (3) are linearly correlated with the time  $\tau$ , the rate constants ( $k_1$ ,  $k_2$ ) can be derived from the slopes of the linear graphs.  $k_{\text{mixed}}$  can be obtained when  $g_{F_g}(X)$  and  $p_{F_g}(X)$  have a linear relationship with time at the same time.

The reduction stage can be divided into the initial stage, in which hematite is reduced to wustite (R.D < 33%), and the mid-term stage, in which wustite is reduced to metallic iron (R.D > 33%). The apparent mixed control rate constants were calculated for both stages and are shown in Figure 4. The metastable samples are reduced at significantly faster rates than the equilibrium samples. The equilibrium samples show a constant reduction rate regardless of the amount of  $\text{Al}_2\text{O}_3$  at the initial stage of reduction, whereas the reduction rate decreases with increasing amounts of  $\text{Al}_2\text{O}_3$  after the mid-term stage. In the metastable samples, the reduction rates are constant up to 2.5 mass% of  $\text{Al}_2\text{O}_3$  content and then increase with the  $\text{Al}_2\text{O}_3$  content as the  $\text{Al}_2\text{O}_3$  content is increased beyond 2.5 mass%.

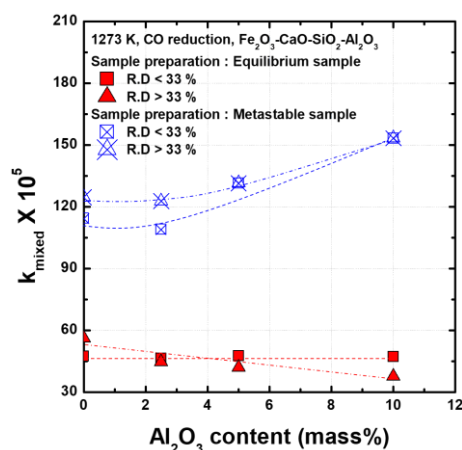
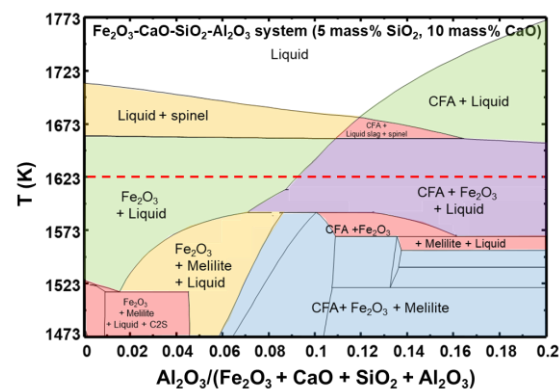


Figure 4. Apparent mixed control rate constants for reduction of  $\text{Fe}_2\text{O}_3$ -CaO-SiO<sub>2</sub>-Al<sub>2</sub>O<sub>3</sub> compacts with various  $\text{Al}_2\text{O}_3$  contents at 1273 K under CO gas.

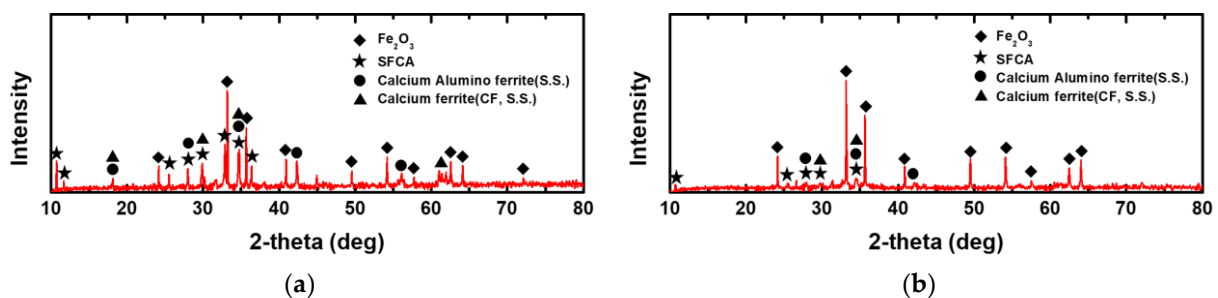
### 3.2. Influence of $\text{Al}_2\text{O}_3$ on the Equilibrium Sample

Figure 5 shows the quaternary phase diagram of  $\text{Fe}_2\text{O}_3$ -CaO-SiO<sub>2</sub>-Al<sub>2</sub>O<sub>3</sub> with 5 mass% SiO<sub>2</sub> and 10 mass% CaO calculated using Factsage 8.0 (Using database of FactPS, FToxide, FTmisc and  $P_{\text{O}_2} = 0.21$ ). The  $\text{Fe}_2\text{O}_3$  and liquid phases coexist at the typical sintering temperature of 1623 K. According to Patrick et al. [12], the SFCA phase forms a liquid phase at 1513 K, and the amount of liquid increases with the temperature. Figure 5 shows that the fraction of the liquid phase increases and that of the  $\text{Fe}_2\text{O}_3$  phase decreases with increasing  $\text{Al}_2\text{O}_3$  content. This suggests that the SFCA phase in the sinter may increase with the  $\text{Al}_2\text{O}_3$  content after quenching. In addition, the CFA,  $\text{Fe}_2\text{O}_3$ , and liquid phases coexist at 9 mass%  $\text{Al}_2\text{O}_3$ . The liquid phase decreases with increasing  $\text{Al}_2\text{O}_3$  content because of the formation of the CFA phase.



**Figure 5.** Quaternary phase diagram of  $\text{Fe}_2\text{O}_3\text{-CaO-SiO}_2\text{-Al}_2\text{O}_3$  with 5 mass%  $\text{SiO}_2$  and 10 mass%  $\text{CaO}$  calculated by Factsage 8.0.

The phase constitutions in the equilibrium and metastable samples were analyzed by XRD, and the results are shown in Figure 6. In both the equilibrium and metastable samples,  $\text{Fe}_2\text{O}_3$ , SFCA, calcium aluminoferrite (S.S), and calcium ferrite (CF, S.S) phases were formed. The metastable process resulted in the formation of more unreacted hematite, and decreased amounts of the SFCA, calcium aluminoferrite, and CF phases.

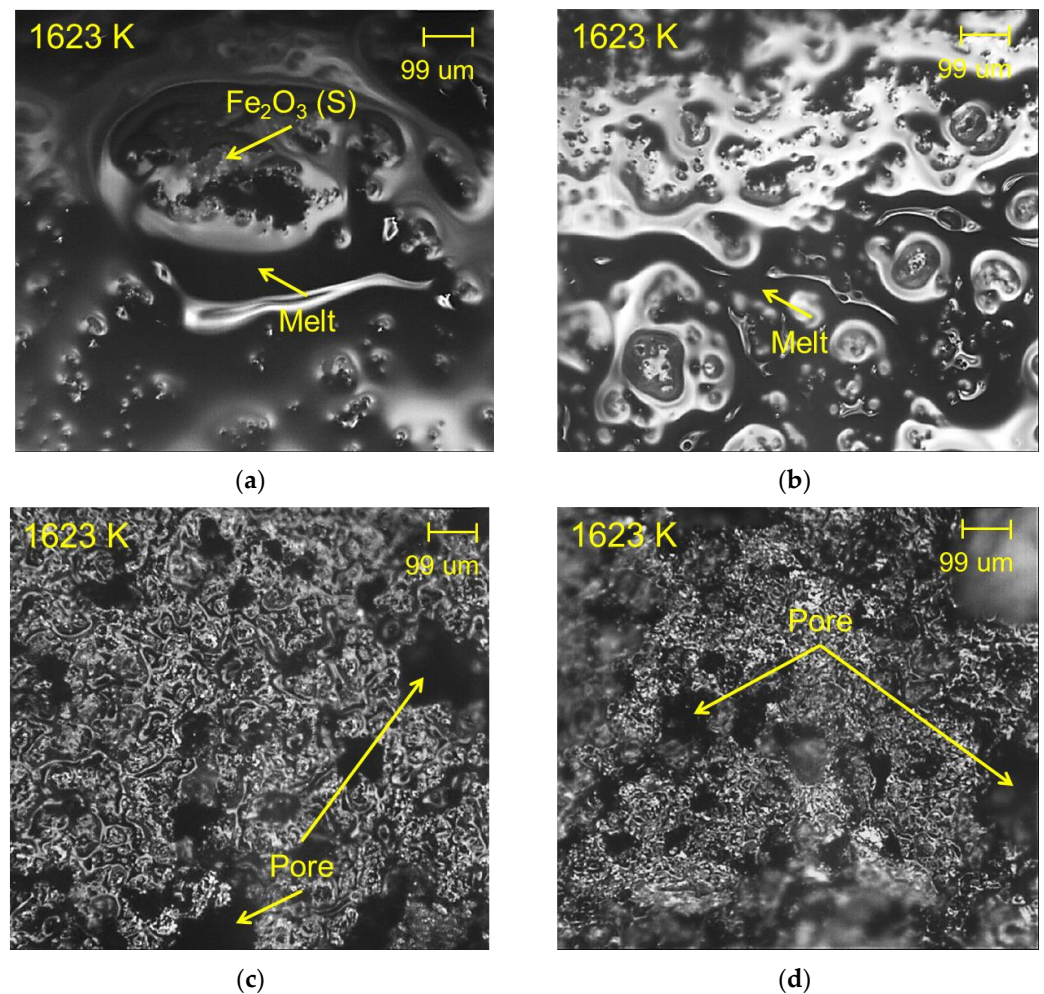


**Figure 6.** XRD analysis of  $\text{Fe}_2\text{O}_3\text{-CaO-SiO}_2\text{-10 mass% Al}_2\text{O}_3$  compacts before reduction: (a) equilibrium sample, (b) metastable sample.

The reduction rates of the equilibrium samples in Figure 4 are constant up to 33% R.D., at which hematite is reduced to wustite. The constant reduction rate is due to the preferential reduction of hematite in the samples at the initial stage of reduction.

The SFCA phase is subsequently reduced after the hematite in the samples has been reduced. According to Liao and Guo [17], because the iron oxide in the SFCA phase has a lower reactivity than hematite, the SFCA phase is reduced at a slower rate than hematite. Therefore, the increased formation of the SFCA phase due to the addition of  $\text{Al}_2\text{O}_3$  in the sample decreases the reduction rate. In contrast, in the metastable samples, the reduction rate increases with the  $\text{Al}_2\text{O}_3$  content regardless of the thermodynamic factors.

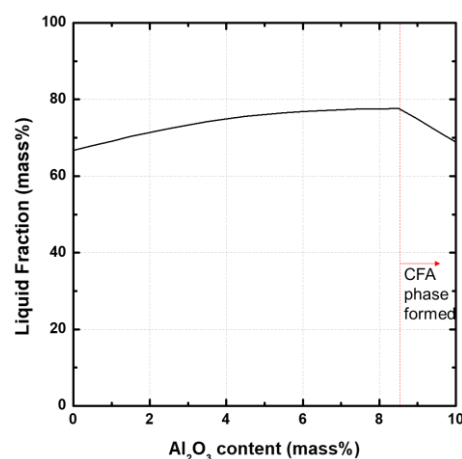
To elucidate the effect of  $\text{Al}_2\text{O}_3$  on the reduction behavior of the metastable samples, the sinter morphology was observed in situ. Liquid phase formation and microstructure changes at high temperature (1623 K) were observed by CLM during the preparation of the metastable  $\text{Fe}_2\text{O}_3\text{-CaO-SiO}_2\text{-Al}_2\text{O}_3$  sample. When  $\text{Al}_2\text{O}_3$  was not added (Figure 7a), the surface of the sample was mostly covered with the liquid phase, and hematite particles were present between the liquid phase. In the 2.5 mass%  $\text{Al}_2\text{O}_3$  sample (Figure 7b), a considerable amount of liquid phase was formed on the surface of the sample, and hematite particles were present between the liquid phase. However, in the 5 mass%  $\text{Al}_2\text{O}_3$  sample (Figure 7c), the fraction of the liquid phase was remarkably decreased, and large-sized pores were observed on the surface of the sample. In the 10 mass%  $\text{Al}_2\text{O}_3$  sample (Figure 7d), there was a larger decrease in the liquid phase, and significant numbers of pores were formed.



**Figure 7.** In situ observation of metastable sample morphology at 1623 K by CLM: (a) 0 mass% Al<sub>2</sub>O<sub>3</sub>, (b) 2.5 mass% Al<sub>2</sub>O<sub>3</sub>, (c) 5 mass% Al<sub>2</sub>O<sub>3</sub>, (d) 10 mass% Al<sub>2</sub>O<sub>3</sub>.

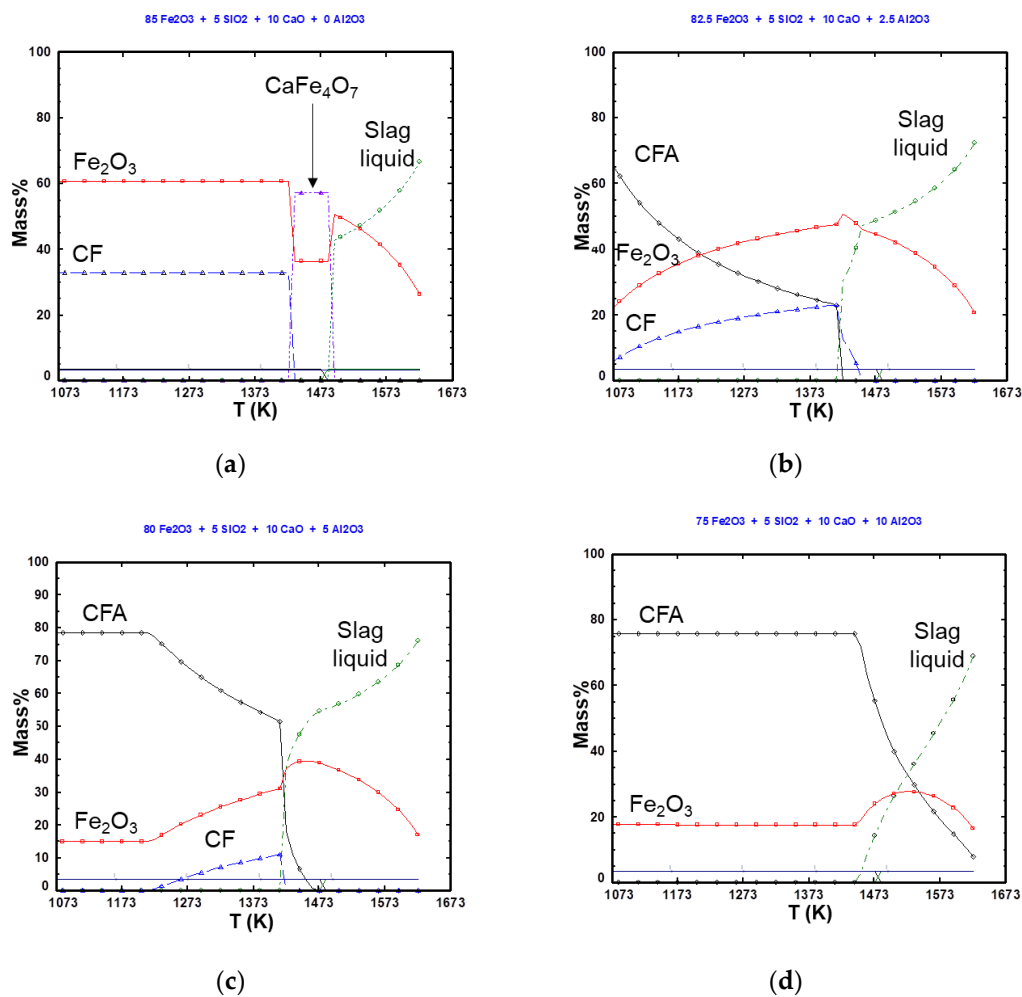
### 3.3. Influence of Al<sub>2</sub>O<sub>3</sub> on the Metastable Sample

Figure 8 shows the variation of the liquid phase fraction with the amount of added Al<sub>2</sub>O<sub>3</sub> in the Fe<sub>2</sub>O<sub>3</sub>-CaO-SiO<sub>2</sub>-Al<sub>2</sub>O<sub>3</sub> system (with 10 mass% CaO and 5 mass% SiO<sub>2</sub>) in the equilibrium state calculated by Factsage 8.0 (Using database of FactPS, FToxide, FTmisc and  $P_{O_2} = 0.21$ ). In the absence of Al<sub>2</sub>O<sub>3</sub>, the fraction of the liquid phase is approximately 65%. As the amount of Al<sub>2</sub>O<sub>3</sub> increases, the fraction of the liquid phase increases to approximately 78%. When the amount of Al<sub>2</sub>O<sub>3</sub> added increases from approximately 8.4 mass% to 10 mass%, the fraction of the liquid phase decreases from approximately 78% to 70%. This decrease in the liquid phase due to the addition of Al<sub>2</sub>O<sub>3</sub> in the high Al<sub>2</sub>O<sub>3</sub> regime has been confirmed in the previous equilibrium phase diagram (Figure 5). The decrease is due to the reaction of the added Al<sub>2</sub>O<sub>3</sub> with Fe<sub>2</sub>O<sub>3</sub> and CaO to form a solid CFA phase. However, in the metastable samples, unlike the equilibrium state, the liquid phase fraction decreases by the addition of Al<sub>2</sub>O<sub>3</sub>, and it is judged that the samples do not follow the formation of the liquid phase behavior in the equilibrium state.



**Figure 8.** Variation of the liquid phase fraction with the Al<sub>2</sub>O<sub>3</sub> added in the Fe<sub>2</sub>O<sub>3</sub>-CaO-SiO<sub>2</sub>-Al<sub>2</sub>O<sub>3</sub> system (with 10 mass% CaO and 5 mass% SiO<sub>2</sub>) in the equilibrium state calculated by Factsage 8.0.

The variation of the equilibrium phase fraction in the Fe<sub>2</sub>O<sub>3</sub>-CaO-SiO<sub>2</sub>-Al<sub>2</sub>O<sub>3</sub> system with the temperature was calculated using Factsage 8.0 (Using database of FactPS, FToxide, FTmisc and  $P_{O_2} = 0.21$ ), and the results are shown in Figure 9. In the Fe<sub>2</sub>O<sub>3</sub>-CaO-SiO<sub>2</sub> system, the Fe<sub>2</sub>O<sub>3</sub> and CF phases coexist at a relatively low temperature, and a CF<sub>2</sub> phase is formed by increasing the temperature. At the sintering temperature of 1623 K, Fe<sub>2</sub>O<sub>3</sub> coexists with liquid slag. When 2.5 mass% Al<sub>2</sub>O<sub>3</sub> is added, the CFA, Fe<sub>2</sub>O<sub>3</sub>, and CF phases coexist. As the temperature increases, the CFA phase fraction decreases, and the Fe<sub>2</sub>O<sub>3</sub> and CF phase fractions increase. At temperatures above 1418 K, the CF and CFA phases rapidly decrease, and liquid slag is formed. When 5 mass% Al<sub>2</sub>O<sub>3</sub> is added, the CF phase is suppressed by Al<sub>2</sub>O<sub>3</sub>, and the CFA phase fraction formed decreases as the temperature increases. In this system, the CFA and CF phases are also rapidly reduced at 1418 K, and a liquid slag phase is formed. When 10 mass% Al<sub>2</sub>O<sub>3</sub> is added, only the CFA and Fe<sub>2</sub>O<sub>3</sub> phases exist prior to liquid formation. In the 0 mass% and 2.5 mass% Al<sub>2</sub>O<sub>3</sub> metastable samples, in which a large amount of liquid is formed, relatively large amounts of the CF phase exist before the liquid slag is formed. In the 5 mass% and 10 mass% Al<sub>2</sub>O<sub>3</sub> metastable samples, which have a smaller amount of liquid phase, the CF phase exists at a very small fraction or is not present before the formation of the liquid slag phase. The main constituent is the CFA phase. Therefore, the liquid phase exists in proportion to the CF phase present. The formation of the CF phase is suppressed by the addition of Al<sub>2</sub>O<sub>3</sub>, while the formation of the liquid phase is decreased by the formation of the CFA phase. According to Guo et al. [21], in the Fe<sub>2</sub>O<sub>3</sub>-CaO system, the CF phase is formed during the sintering process, whereas in the Fe<sub>2</sub>O<sub>3</sub>-CaO-Al<sub>2</sub>O<sub>3</sub> system, the CF phase decreases with the addition of Al<sub>2</sub>O<sub>3</sub> and the CFA phase is formed. It was reported that when more than approximately 4.76 mass% Al<sub>2</sub>O<sub>3</sub> is added, all the CF is exhausted, and the CFA phase is present. In addition, according to Bai et al. [22], as the Al<sub>2</sub>O<sub>3</sub> content increases from 1.4% to 2.8%, the total amount of CF decreases slightly. When the Al<sub>2</sub>O<sub>3</sub> content is greater than 2.8%, the CF content significantly decreases with increasing Al<sub>2</sub>O<sub>3</sub> content. Despite the slight differences in the amounts of Al<sub>2</sub>O<sub>3</sub>, the overall trend is consistent with the results of this experiment and those from other researchers. Therefore, as the amount of the liquid formed decreases, the number of pores in the metastable sample increases, which affects the reduction rate.



**Figure 9.** Variation of the equilibrium phase fractions in the  $\text{Fe}_2\text{O}_3$ -CaO-SiO<sub>2</sub>-Al<sub>2</sub>O<sub>3</sub> system with the temperature, calculated using Factsage 8.0: (a) 0 mass% Al<sub>2</sub>O<sub>3</sub>, (b) 2.5 mass% Al<sub>2</sub>O<sub>3</sub>, (c) 5 mass% Al<sub>2</sub>O<sub>3</sub>, and (d) 10 mass% Al<sub>2</sub>O<sub>3</sub>.

The GMT rate constants (R.D > 33% region) were derived from the results of this experiment, and the results of the porosity analysis on the sample prior to reduction are shown in Figure 10. In the equilibrium samples, the GMT rate constant does not change significantly with the addition of Al<sub>2</sub>O<sub>3</sub>, whereas in the metastable samples, the GMT rate constant is constant up to 2.5 mass% of Al<sub>2</sub>O<sub>3</sub> and increases significantly above 5 mass% of Al<sub>2</sub>O<sub>3</sub>. The reduction rate of the metastable samples is proportional to the porosity of the sample. The porosity has a similar value to that of the equilibrium sample and remains constant up to the addition of 2.5 mass% of Al<sub>2</sub>O<sub>3</sub>; however, when 5 mass% or more Al<sub>2</sub>O<sub>3</sub> is added, the porosity tends to increase significantly. The change in porosity with the addition of Al<sub>2</sub>O<sub>3</sub> is closely related to the amount of liquid formed during sample preparation. The porosity and amount of liquid formed tend to be inversely proportional to each other. The changes in the porosity with the addition of Al<sub>2</sub>O<sub>3</sub> are consistent with the results of other works [19,23]. The metastable samples show a tendency for increased reduction rates despite the lowering of the iron oxide reactivity by the formation of the SFCA phase due to Al<sub>2</sub>O<sub>3</sub>. Therefore, in determining the reduction rate of the sinter, the influence of the microstructure on the diffusion of the reducing gas is more significant than that of the ICR due to the formation of the SFCA phase. Kato et al. [24] and Harvey et al. [25] have also reported that the microstructure is a more important influencing factor than the iron oxide reactivity in sinter reduction.

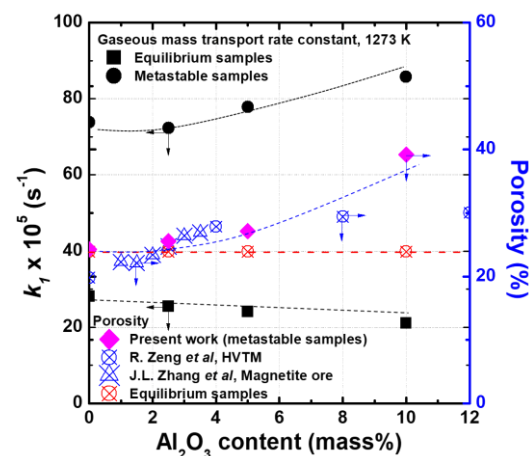


Figure 10. Variation of apparent GMT rate constant and sinter porosity with  $\text{Al}_2\text{O}_3$  content.

#### 4. Conclusions

To understand the effect of  $\text{Al}_2\text{O}_3$  on the sinter, equilibrium samples and metastable samples were prepared, and reduction experiments were conducted at 1273 K using CO gas. As the  $\text{Al}_2\text{O}_3$  content increased, the initial reduction rate of the equilibrium samples remained constant, but the reduction rate tended to decrease in proportion to the amount of  $\text{Al}_2\text{O}_3$  added after the mid-term stage of reduction. The metastable samples showed a constant reduction rate with the addition of up to 2.5 mass%  $\text{Al}_2\text{O}_3$  and an increased reduction rate when more than 5 mass%  $\text{Al}_2\text{O}_3$  was added. The equilibrium samples exhibited a constant reduction rate due to the reduction of hematite in the initial stage of reduction, but after the hematite was exhausted in the mid-term stage of reduction and the formation of the SFCA phase by  $\text{Al}_2\text{O}_3$  became the main reduction target, the reduction rate decreased. The formation of the SFCA phase due to the addition of  $\text{Al}_2\text{O}_3$  was also confirmed in the metastable samples. However, the formation of pores changed the microstructure of the samples significantly. The porosity was constant with the addition of up to 2.5 mass%  $\text{Al}_2\text{O}_3$  and increased significantly when more than 5 mass%  $\text{Al}_2\text{O}_3$  was added. These trends in the porosity are closely related to liquid phase formation during the sample preparation process. The reduction behavior of the metastable samples tends to match the changes in porosity. Therefore, in determining the reduction rate in the sinter, the influence of the microstructure on the diffusion of the reducing gas is more important than the influence of the ICR caused by the formation of the SFCA phase.

**Author Contributions:** Writing—Original draft preparation, S.G.S. and W.H.K.; writing—Review and editing, D.J.M. All authors have read and agreed to the published version of the manuscript.

**Funding:** This research received no external funding.

**Institutional Review Board Statement:** Not applicable.

**Informed Consent Statement:** Not applicable.

**Data Availability Statement:** Data sharing not applicable.

**Acknowledgments:** This work was supported by the Korea Institute of Energy Technology Evaluation and Planning (KETEP) and the Ministry of Trade, Industry & Energy (MOTIE) of the Republic of Korea (No. 20172010106300) and the Korea Evaluation Institute of Industrial Technology (No. 10076604).

**Conflicts of Interest:** The authors declare no conflict of interest.

## References

1. Fernández-González, D.; Ruiz-Bustanza, I.; Mochón, J.; González-Gasca, C.; Verdeja, L.F. Iron ore sintering: Quality indices. *Miner. Process. Extra. Metall. Rev.* **2017**, *38*, 254–264. [[CrossRef](#)]
2. Fernández-González, D.; Ruiz-Bustanza, I.; Mochón, J.; González-Gasca, C.; Verdeja, L.F. Iron ore sintering: Raw materials and granulation. *Miner. Process. Extra. Metall. Rev.* **2017**, *38*, 36–46. [[CrossRef](#)]
3. Hino, M.; Nagasaka, T.; Katsumata, A.; Higuchi, K.-I.; Yamaguchi, K.; Kon-No, N. Simulation of primary-slag melting behavior in the cohesive zone of a blast furnace, considering the effect of  $\text{Al}_2\text{O}_3$ ,  $\text{Fe}_t\text{O}$ , and basicity in the sinter ore. *Metall. Mater. Trans. B* **1999**, *30*, 671–683. [[CrossRef](#)]
4. Wu, S.; Huang, W.; Kou, M.; Liu, X.; Du, K.; Zhang, K. Influence of  $\text{Al}_2\text{O}_3$  Content on Liquid Phase Proportion and Fluidity of Primary Slag and Final Slag in Blast Furnace. *Steel Res. Int.* **2015**, *86*, 550–556. [[CrossRef](#)]
5. Das, S.K.; Das, B.; Sakthivel, R.; Mishra, B.K. Mineralogy, Microstructure, and Chemical Composition of Goethites in Some Iron Ore Deposits of Orissa. India. *Miner. Process. Extra. Metall. Rev.* **2010**, *31*, 97–110. [[CrossRef](#)]
6. Wu, S.; Zhai, X. Factors influencing melt fluidity of iron ore. *Metall. Res. Technol.* **2018**, *115*, 505. [[CrossRef](#)]
7. Kasai, E.; Sakano, Y.; Nakamura, T. Influence of Iron Ore Properties on the Flow of Melt Formed in the Sintering Process. *Tetsu Hagane* **2000**, *86*, 139–145. [[CrossRef](#)]
8. Lu, L.; Holmes, R.J.; Manuel, J.R. Effects of Alumina on Sintering Performance of Hematite Iron Ores. *ISIJ Int.* **2007**, *47*, 349–358. [[CrossRef](#)]
9. Zhang, G.-L.; Wu, S.-L.; Su, B.; Que, Z.-G.; Hou, C.-G.; Jiang, Y. Influencing factor of sinter body strength and its effects on iron ore sintering indexes. *Int. J. Miner. Metall. Mater.* **2015**, *22*, 553–561. [[CrossRef](#)]
10. Hsieh, L.-H.; Whiteman, J.A. Sintering conditions for simulating the formation of mineral phases in industrial iron ore sinter. *ISIJ Int.* **1989**, *29*, 24–32. [[CrossRef](#)]
11. Kim, H.; Park, J.; Cho, Y. Crystal structure of calcium and aluminium silicoferrite in iron ore sinter. *Ironmak. Steelmak.* **2002**, *29*, 266–270. [[CrossRef](#)]
12. Patrick, T.R.; Pownceby, M.I. Stability of silico-ferrite of calcium and aluminum (SFCA) in air-solid solution limits between 1240 C and 1390 C and phase relationships within the  $\text{Fe}_2\text{O}_3$ -CaO- $\text{Al}_2\text{O}_3$ - $\text{SiO}_2$  (FCAS) system. *Metall. Mater. Trans. B* **2002**, *33*, 79–89. [[CrossRef](#)]
13. Loo, C.E.; Leung, W. Factors influencing the bonding phase structure of iron ore sinters. *ISIJ Int.* **2003**, *43*, 1393–1402. [[CrossRef](#)]
14. Li, L.; Liu, J.; Wu, X.; Ren, X.; Bing, W.; Wu, L. Influence of  $\text{Al}_2\text{O}_3$  on equilibrium sinter phase in  $\text{N}_2$  atmosphere. *ISIJ Int.* **2010**, *50*, 327–329. [[CrossRef](#)]
15. Heikkinen, E.-P.; Iljana, M.; Fabritius, T. Review on the Phase Equilibria in Iron Ore Sinters. *ISIJ Int.* **2020**, *60*, 2633–2648. [[CrossRef](#)]
16. Mazanek, E.; Jasienska, S. Formation of binary ferrites in iron ore sinters. *Iron Stell Inst. J.* **1966**, *204*, 344–348.
17. Liao, F.; Guo, X.-M. Effect of aluminum content on reduction of silico-ferrite of calcium and aluminum (SFCA). *Mater. Res. Express* **2019**, *6*, 106501. [[CrossRef](#)]
18. Hessien, M.; Kashiwaya, Y.; Ishii, K.; Nasr, M.; El-Geassy, A. Sintering and heating reduction processes of alumina containing iron ore samples. *Ironmak. Steelmak.* **2008**, *35*, 191–204. [[CrossRef](#)]
19. Zeng, R.; Li, W.; Wang, N.; Fu, G.; Chu, M.; Zhu, M. Effect of  $\text{Al}_2\text{O}_3$  on the gas-based direct reduction behavior of Hongge vanadium titanomagnetite pellet under simulated shaft furnace atmosphere. *Powder Technol.* **2020**, *376*, 342–350. [[CrossRef](#)]
20. Szekely, J.; Evans, J.; Sohn, H. *Gas-Solid Reactions*; Academic Press: New York, NY, USA, 1976; pp. 128–131.
21. Guo, H.; Guo, X.M. Effect of alumina on liquid phase formation in sintering process of iron ore fines. *Steel Res. Inter.* **2019**, *90*, 1900138. [[CrossRef](#)]
22. Bai, K.; Shen, J.; Zhu, Z.; Zuo, H.; Pan, Y.; Wang, J.; Xue, Q. Effect of  $\text{Al}_2\text{O}_3$  on the Formation of Calcium Ferrite in the Solid State. *Metals* **2019**, *9*, 681. [[CrossRef](#)]
23. Zhang, J.-L.; Wang, Z.-T.; Xing, X.-D.; Liu, Z.-J. Effect of aluminum oxide on the compressive strength of pellets. *Int. J. Min. Met. Mater.* **2014**, *21*, 339–344. [[CrossRef](#)]
24. Kato, K.; Konishi, H.; Ono, H.; Fujimoto, S.; Koizumi, Y. Influence of CaO/ $\text{SiO}_2$  on the Reduction Behavior of Sintered  $\text{Fe}_2\text{O}_3$ -CaO- $\text{SiO}_2$ - $\text{Al}_2\text{O}_3$  Tablets at the Softening and Melting Temperatures. *ISIJ Int.* **2020**, *60*, 1479–1786. [[CrossRef](#)]
25. Harvey, H.; Pownceby, M.I.; Chen, J.; Webster, N.A.S.; Nguyen, T.B.T.; Matthews, L.; O’dea, D.; Honeyands, T. Effect of Temperature, Time, and Cooling Rate on the Mineralogy, Morphology, and Reducibility of Iron Ore Sinter Analogues. *JOM* **2021**, *73*, 345–355. [[CrossRef](#)]